Journal of Materials Chemistry A

ROYAL SOCIETY OF CHEMISTRY

COMMUNICATION

View Article Online
View Journal | View Issue

Cite this: J. Mater. Chem. A, 2025, 13, 3273

Received 10th October 2024
Accepted 7th January 2025

DOI: 10.1039/d4ta07239a

rsc.li/materials-a

Microtextured coatings from superhydrophobic bark-derived bioparticles for fog harvesting†

Sameer Mhatre, *[ab] Xun Niu[ab] and Orlando Rojas *[abcd]

We have developed bioparticle-based hybrid superhydrophobic–hydrophilic coatings that significantly enhance water collection in fog harvesting. The use of superhydrophobic betulin crystals, extracted from birch bark, to create microtextured coatings represents a sustainable and superior alternative to synthetic nano/micro patterning. These betulin coatings effectively accelerate condensation and coalescence of water microdroplets, leading to considerable drop growth and water collection. The surface energy heterogeneity, with a hydrophilic substrate surrounding the superhydrophobic bioparticles, creates a surface free energy gradient that substantially enhances droplet mobility. Notably, we observed a non-monotonic increase in condensation and water collection rates with surface particle density. Through rigorous testing on both permeable and impermeable substrates, we found that the water collection efficiency of betulin-coated surfaces far surpasses that of bare substrates. Further, the betulin-based collectors increased the efficiency of widely-used fog harvesters like Raschel meshes by up to 275%. Compared to previously reported biomimetic microtextured surfaces, our betulin-based collectors demonstrate unparalleled water harvesting capabilities, signaling a breakthrough in environmentally friendly patterning for water condensation and harvesting.

1 Introduction

In response to changing weather patterns aggravated by climate change, there is an increasing need to find reliable water sources in various parts of the world, particularly in arid regions. People in these traditionally dry areas are continually seeking new ways to harvest water from local resources. Methods such as seawater desalination, water reclamation, and fog harvesting are being employed to address this challenge. In water-scarce areas like mountaintops, desert coastal regions, and arid areas, the air is rich in moisture and fog is prevalent.[1] Taking cues from nature, bio-mimetic techniques have a long history of being used to harvest water from the air to meet human needs. The amount of water harvested has been reported to be sufficient for daily human and animal consumption, as well as for supporting reforestation efforts.[2] Furthermore, this approach has proven beneficial in capturing water in industrial processes, including cooling towers and thermal power plants.[3]

Improving traditional water harvesting methods is a desirable goal, which can be achieved by modifying the collection material or improving aerodynamics. Many studies have focused on the geometric aspects of fog collectors,[4] highlighting geometries such as metal meshes and vertical metal wire "harps"[5] as more efficient than flat metal sheets.[6] However, each system has its drawbacks; for instance, fine meshes are prone to clogging, and wider meshes struggle to effectively trap tiny water droplets. Due to aerodynamic reasons, permeable collectors like meshes are considered more efficient than impermeable sheets.[6,7] Nonetheless, regardless of the design, not all water passing through a mesh is collected.[4]

A fog collector serves as an effective method for water condensation and droplet anchorage due to its large surface area. Additionally, water collection can occur through drop nucleation and growth as a result of condensation and surface coalescence. The use of hydrophobic surfaces intensifies condensation,[8] allowing water drops to grow and roll down, which in turn creates space for fresh nucleation and drop growth. Water condensation can take place in either a drop-wise or film-wise manner,[9] with the former being preferred[10] for its greater heat transfer rate and the continuous clearing of surface area by falling larger drops, enabling new nucleation and droplet growth.[11,12] Recent studies have been focused on improving drop-wise condensation by enhancing surface

[a]BioProducts Institute, University of British Columbia, Vancouver, V6T 1Z4, BC, Canada. E-mail: sameer.mhatre@ubc.ca; orlando.rojas@ubc.ca
[b]Department of Chemical and Biological Engineering, University of British Columbia, Vancouver, V6T 1Z3, BC, Canada
[c]Department of Chemistry, University of British Columbia, Vancouver, V6T 1Z1, BC, Canada
[d]Department of Wood Science, University of British Columbia, Vancouver, V6T 1Z4, BC, Canada

† Electronic supplementary information (ESI) available. See DOI: https://doi.org/10.1039/d4ta07239a

hydrophobicity[13] or utilizing hybrid superhydrophobic–superhydrophilic surfaces.[14]

The water collection efficiency in fog harvesting is governed by several factors such as fog droplet number density, droplet size, wind speed, and mesh geometry.[2] Recently special attention has been paid to surface characteristics of the fog harvester. Several bio-mimetic surfaces have been proposed to augment the water condensation and coalescence in comparison with the untreated surfaces.[15] For example, a spider network-like structure made of poly(methyl methacrylate) (PMMA)-coated nylon filaments was found to amplify surface water coalescence.[16] Further, a roughness gradient on the filaments, similar to a cactus spine, drives adjacent droplets closer, which eventually coalesce and fall after growing big.[17,18] A similar effect can be attained by the periodic spindle-knot structures found on cribellate spider web.[19,20] Some desert species, *e.g.*, *Stenocara* beetles extract water from the moist air through tiny bumps on their back, which inspired scientific studies on the condensation on macro-patterned surfaces with hydrophobic–hydrophilic patches.[21–23] Various techniques have been employed to attain such nano/micro-structured surfaces,[13] including laser irradiation patterning,[22] electrochemical deposition,[24] photocatalytic lithography,[25] electrophoretic deposition[26] and chemical etching.[27] The superhydrophobic surfaces are reported to exhibit pinning of droplets, ascribed to the nucleation between the features, which inhibit drop shedding. An enduring pinning can be mitigated by hydrophilic-hydrophobic surfaces where the Cassie state prevails. However, micropatterning is not feasible in fog harvesting applications, primarily due to the economical and technical reasons, associated with the large surface areas involved and the flexibility of the collectors. Moreover, synthetic materials[13] used to achieve the patterns are not environmentally friendly and sustainable, given limited resources and poor biodegradability after the end of service life. Examples of the materials used to achieve superhydrophobicity include Titania,[28] heptadecafluorodecyl-trimethoxysilane,[29] carbon nanotubes, microstructured gold surfaces with thiols,[25] *etc.*

We are presenting an innovative approach using plant-based colloids, specifically betulin particles, to engineer a range of surface morphologies with superhydrophobic–hydrophilic characteristics. Betulin particles, obtained from birch bark, exhibit inherent superhydrophobic properties. Unlike synthetic compounds such as paraffin waxes and fluorinated silanes used for creating superhydrophobic surfaces,[14,30,31,33] betulin particles are cost-effective, sustainable, and environmentally friendly, making them suitable for application in commercial fog harvesters. Our proposed microstructures, featuring superhydrophobic betulin particles on hydrophilic substrates, enable the development of surface free energy gradients, leading to enhanced condensation and mobility of the water microdroplets. Our observations highlight the significant impact of surface composition on these phenomena, as evidenced by our experimentation with impermeable substrates like glass to determine the most effective composition for water collection. We then proceeded to apply these findings to commercial meshes utilized in fog harvesting.

2 Materials and methods

2.1 Betulin particles

Betulin particles were Soxhlet extracted from birch bark. A detailed method of extraction is previously reported,[52–54] which is also presented in the ESI.† The resulting extractives contained 95% betulin crystals. The rice grain-shaped particles, shown in Fig. S1,† were 5.6 ± 0.8 μm long and 1.6 ± 0.4 μm wide.

2.2 Binders and coating application methods

The particles were bound to the substrates using linseed oil (Grumbacher, USA) and polylactic acid (NatureWorks, USA) as binders. These plant-based binders were chosen for their biodegradability and non-toxic properties, ensuring that their breakdown or release at the end of the coating's life cycle would not contaminate water or land. Linseed oil was used as is, while PLA was dissolved in dichloromethane and ethyl acetate to create two different types of coatings. The betulin particles were mixed with the binder mixture using an ultrasonic probe sonicator (Sonifier SFX550, Branson Ultrasonics, USA) under sonication. The two-step process of the mixture preparation is illustrated in Fig. 1(a and b).

The betulin mixtures were applied to the impermeable substrate, *i.e.*, glass using spin as well as rod coating methods, whereas the meshes were coated using spray coating as demonstrated in Fig. 1(c). The betulin coatings applied to glass substrates were primarily studied to explore condensation and water collection efficiencies. The observations were applied to two meshes; (1) stainless steel SS304 wire mesh (12 holes per linear inch, 1.58 mm aperture, 0.6 mm wire diameter), and (2) 35% Raschel mesh.

2.3 Static and roll-off contact angle measurements

The contact angle (θ) measurements were done using a tensiometer (Thetaflex 300, Biolin Scientific). The water and diiodomethane droplets used in contact angle measurements were 5 μL in size, while some roll-off angle measurements were done with 30 μL drops. The roll-off angle measurements were done by tilting the substrate at 30° min^{-1}. All measurements were done in air at room temperature.

2.4 Surface free energy measurement

The Owens–Wendt–Rabel and Kaelble (OWRK) model[32] was used to estimate the overall surface free energy (γ_s) of the betulin coatings.

$$\sqrt{\Gamma_s^d \gamma_l^d} + \sqrt{\Gamma_s^p \gamma_l^p} = \frac{\gamma_l(1+\cos\theta)}{2} \quad (1)$$

The superscripts d and p indicate dispersive and polar components of surface tension (γ_l) and surface free energy (Γ_s). The surface tension and contact angle on a substrate were measured for two liquids *i.e.* diiodomethane (Sigma Aldrich) and de-ionized water, polar and dispersive interactions of which were known. The unknowns Γ_s^d and Γ_s^p were obtained by simultaneous solution of eqn (1), applied to diiodomethane and water, where their sum corresponds to the surface free energy Γ.

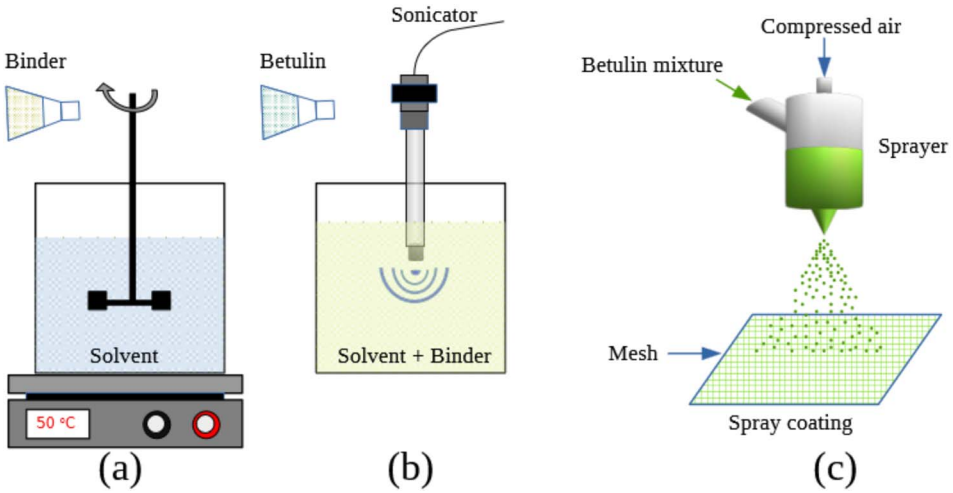

Fig. 1 Schematic illustrations showing the preparation of betulin mixtures and the application of coatings on mesh collectors. (a) A binder is dissolved in a solvent at 50 oC while stirring (linseed oil-based coatings did not require this step). (b) Betulin is mixed into the binder solution using a probe solicitor at room temperature. (c) The betulin coatings are applied to the mesh-type fog harvester using spray coating.

2.5 Surface morphology and condensation imaging

The microtexture of the coatings was examined using scanning electron microscopy (Helios NanoLab 650). A coating to be imaged was deposited on $a \approx 150$ μm thick glass which was further covered with a 10 nm iridium layer using a coating system (Leica EM MED020). The imaging was done at 5 to 15 kV acceleration voltage.

The mobility of condensed microdroplets on the betulin coating surfaces was estimated by capturing droplets at 50 frames per second under the Olympus BX53 optical microscope. The substrate was positioned horizontally on the microscope stage. Care was taken to ensure that it was perfectly level. Subsequently, it was exposed to the humidifier for a brief duration, and it is important to note that no coolant was passed through during this process. The image analysis tool ImageJ was used to estimate the time-averaged surface motion of the microdroplets.

2.6 Water collection rate measurement

The water collection rates were measured on 7.5 cm × 2.6 cm impermeable samples and 10 × 10 cm^2 impermeable (*i.e.* mesh) samples. The atmospheric conditions were manipulated to create a dense fog at a temperature of 22 °C. This fog, generated with the help of an acoustic humidifier, having a high relative humidity of 90%. The fog also contained an abundance of microdroplets, measuring below 25 μm in diameter. The fog was directed to a collector sample, which was held at 45° to minimize the aerodynamic resistance to the fog by the collector and easier shedding of the larger water drops from the collector surface.[55] The water accumulated at the base of the sample was measured after 30 minutes to estimate the time averaged water collection rates.

3 Results and discussion

To adhere betulin particles to a surface, we explored various binders and solvents to achieve the optimal surface texture and water collection efficiency. Our primary focus was on selecting environmentally friendly binders, including plant-based linseed oil, polylactic acid (PLA), and polydimethylsiloxane (PDMS). We formulated PLA-based coatings using dichloromethane (DCM) and ethyl acetate solvents, while isopropanol was used in the PDMS-based mixtures. These solvents were carefully chosen for their ability to dissolve betulin, albeit sparingly. To simplify our terminology, we named the betulin coatings derived from linseed oil, PLA-DCM, PLA-ethyl acetate, and PDMS-isopropanol mixtures as Bet-LO, Bet-PLA-1, Bet-PLA-2, and Bet-PDMS, respectively. Additionally, the term "betulin content" denotes the wt% of the particles in the applied suspensions.

Glass was primarily used as a substrate to study condensation and fog harvesting capabilities of the coatings. The observations established the optimum particle densities in the coatings and their water collection rates using the glass collectors. The identified optimal coatings were then applied to Raschel and stainless steel meshes to assess their practicality in fog harvesting. Different coating application methods were chosen based on the substrate; spin and rod coating for impermeable glass, while spray coating for the meshes.

3.1 Surface microtexture

The surface morphology and betulin particle distribution at the solid–air interface govern the condensation rate, as the microtexture is responsible for wettability and microdroplet mobility on the surface. The binders and solvents used to apply betulin played a crucial role in the morphology development of the resultant coating after the liquid film was dried. For example, the Bet-PLA-1 coatings were porous, where the pore density was increased after the addition of betulin particles, as can be seen in Fig. 2(a)–(c). Without betulin, the PLA coatings contained larger, but widely spaced pores (Fig. 2(a)). However, the addition of a small amount of betulin rendered a pumice stone-like texture to the Bet-PLA-1 coatings (Fig. 2(b)). Further, the increase in the betulin content roughened the surface, where

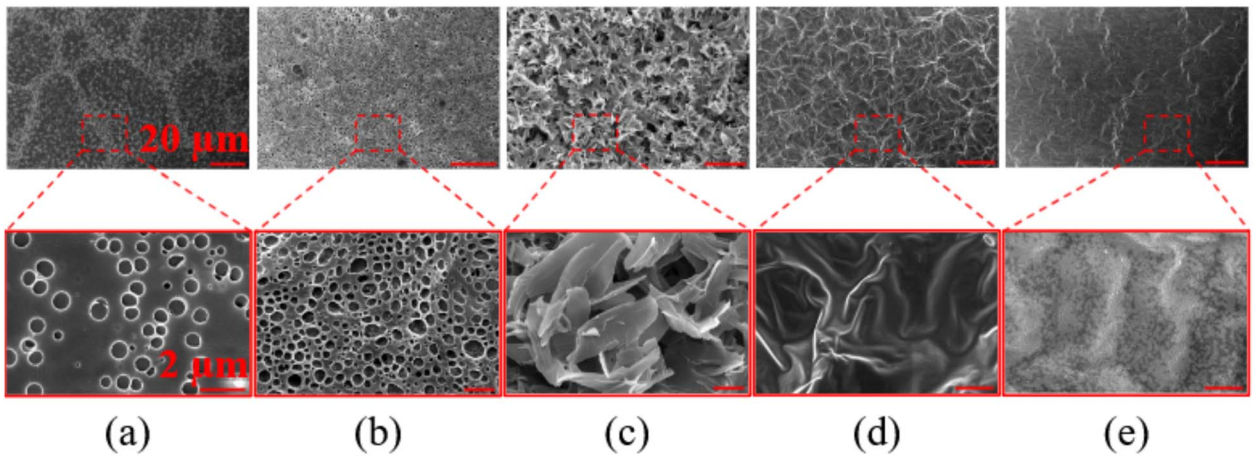

Fig. 2 The scanning electron microscope (SEM) images depicting the effects of binder mixtures on the microtexture of the resultant coatings. The porous surfaces of Bet-PLA-1 coatings made from mixtures containing (a) 0% betulin, (b) 1 wt% betulin, and (c) 5 wt% betulin. The Bet-PDMS (d) and Bet-LO (e) coatings turn wrinkly upon drying.

closely packed particles can be seen in Fig. 2(c). The Bet-PDMS (Fig. 2(d)) and Bet-LO (Fig. 2(e)) coatings, *on the other hand*, shrunk after drying, resulting in wrinkled surfaces.

The porous texture of the PLA-based betulin coatings was mitigated by replacing DCM with ethyl acetate as a solvent. As shown in Fig. 3(a), the resultant coatings were flat, without pores or wrinkles. A typical surface of a Bet-PLA-2 coating was made of randomly oriented sparse rice grain-shaped betulin particles, where the void around the particles was covered with a thin PLA layer. A large density of the particles in a coating was responsible for its surface microroughness. The 5 wt% Bet-PLA-2 coating, shown in Fig. 3(b) and (d), consists of densely packed overlapping particles fully covering the substrate. The individual particles in such coatings were bound to the adjacent particles as well as to the substrate.

3.2 Surface free energies

When exposed to fog, water condenses on the superhydrophobic betulin surface. As the fog also carries water droplets and they land on the surface, they are then pushed to the hydrophilic part along with the condensed microdroplets. The coating surface experiences water droplet growth primarily

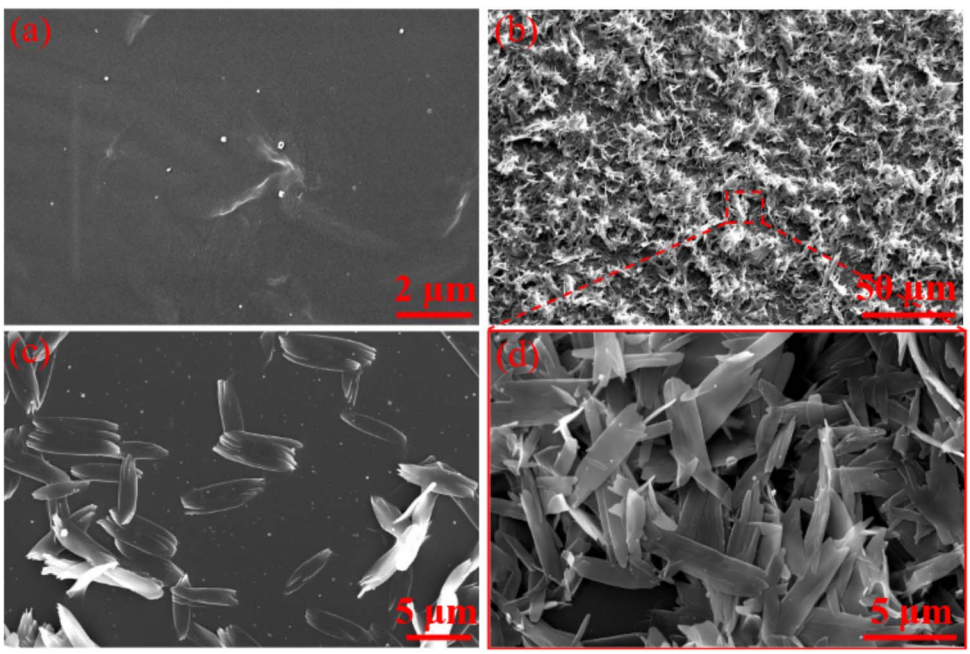

Fig. 3 The SEM images illustrating the microtextures of Bet-PLA-2 coated surfaces, showcasing the different compositions of the coatings. The coatings made with no betulin (a), 5 wt% betulin (b), and 3 wt% betulin (c) mixtures. The zoomed-in section in (d) provides a detailed view of particle assembly in the coating from (b).

through surface coalescence, driven by the mobility of these microdroplets. The surface mobility is attributed to the gradient of the surface free energy ($\Delta\Gamma$) and Laplace pressure (ΔP). As can be seen in Fig. 3(c), and also demonstrated in Fig. 5(a), islets of the superhydrophobic betulin surface are surrounded by the hydrophilic substrate, primarily made of a binder. The distinctive surface free energies of the two, set a water droplet in motion upon coming into contact with the coating.

When the surfaces were fully covered with betulin particles (as shown in Fig. 3(b) and (d)), the Cassie–Baxter state prevailed, where a liquid does not penetrate in-between the particles, also called heterogeneous wetting regime.[34] Although the roughness did not change the surface chemistry of the coatings, the apparent overall surface free energies presented in Fig. 4 clearly demonstrate the effect of betulin content on the wettability of the surfaces and helped to identify its optimum. The surface free energy (Γ) of betulin-coated surfaces are substantially different from a bare glass surface, whereas among the coated surfaces, the data shows a non-monotonic pattern. The overall surface free energies of the Bet-PLA-2 and Bet-LO coatings are presented in Fig. 4(a), along with their polar (Γ^{p}) and dispersive (Γ^{d}) components in Fig. 4(b). On the Bet-PLA-2 coatings, Γ decreased with the increased areal particle density, however, the trend reversed above 4 wt% betulin. The Γ of Bet-LO coatings differ from that of the Bet-PLA-2 and show, albeit a smaller, steady reduction with rising particle density. The changes in Γ with the surface particle densities are attributed to the changes in dispersion force interactions in the respective coatings. The large deviation in the polar and dispersive components is a characteristic of solid–liquid interfaces,[35] suggesting substantially weaker polar interactions. Interestingly, the polar force interactions appear to build up as a result of the excess surface particle density above 4 wt% betulin. The surface free energy data overall indicates that the wettability of a coating dwindles upon increasing its betulin content, where it passes through a minima when the inter-particle separation is optimum.

The distinct wettabilities of a betulin surface and bare glass are also evident from the difference in their water contact angles (WCA). The contact angles on a glass surface and a betulin particle layer were 40° and 156°, respectively. The betulin coatings exhibited hydrophobicity which built up with their particle density. While the presence of betulin in a coating was found to raise the water contact angle significantly, in the Bet-LO coatings an increase in the surface betulin density did not show a noticeable gain in WCA. By contrast, the contact angle on Bet-PLA-1 and Bet-PLA-2 coatings increased with the surface particle density up to a point. The Bet-PLA-2 coatings appeared to become superhydrophobic at betulin content above 3 wt%; however, the large water contact angle can be attributed to the Cassie state due to the surface roughness as demonstrated in Fig. 3(b) and (d) and termed as apparent contact angle.

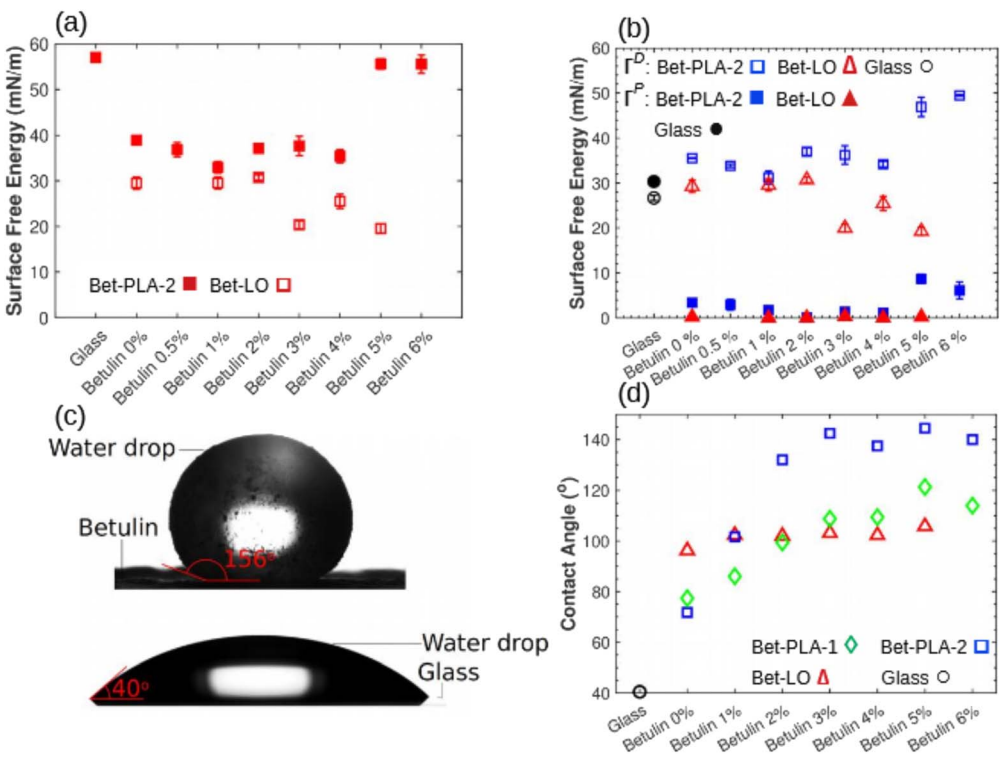

Fig. 4 (a) Overall surface free energies (Γ) on Bet-LO (□) and Bet-PLA-2 (■) coatings. (b) Polar (Γ_P, solid symbols) and dispersive (Γ_D, hollow symbols) components of Γ on the Bet-PLA-2 (blue) and Bet-LO (red) coatings. (c) Water drops on a betulin cake and glass exhibit distinct wetting properties. Some betulin particles from the cake can be observed adhering to the drop surface. (d) Water contact angle on Bet-PLA-1 (◇), Bet-PLA-2 (□), and Bet-LO (△) coatings. The contact angles on the coating with densely packed betulin particles can be treated as apparent contact angles.

3.3 Surface mobility and coalescence of microdroplets

The hybrid nature of the coatings is ascribed to the superhydrophobic betulin surface and hydrophilic surrounding made of a binder. On Bet-LO, Bet-PLA-1, and Bet-PLA-2 surfaces, the maximum water contact angle gradients were 60°, 80° and 85°, respectively. Similarly the surface free energy gradients ($\Delta\Gamma$) on Bet-LO and Bet-PLA-2 surfaces were measured to be $\approx$93 and 83 mN m^{-1}, respectively. As illustrated in Fig. 5(a), the $\Delta\Gamma$ induced the water droplet mobility and coalescence on the betulin-coated surfaces. Any microdroplet formed or settled on a betulin surface is drifted away, towards the particle-free region. The course of a moving droplet is determined by the particles on its way and their orientation. The mobile droplets merge with smaller ones on their path, before drawing off into large stagnant drops. A surface lacking betulin particles behaves like a hydrophilic pool, causing adjacent droplets to converge and merge into larger sizes, subsequently rolling freely on the tilted collector surface.

Moreover, the randomness in the orientation of the particles is attributed to the curvature gradient experienced by a water

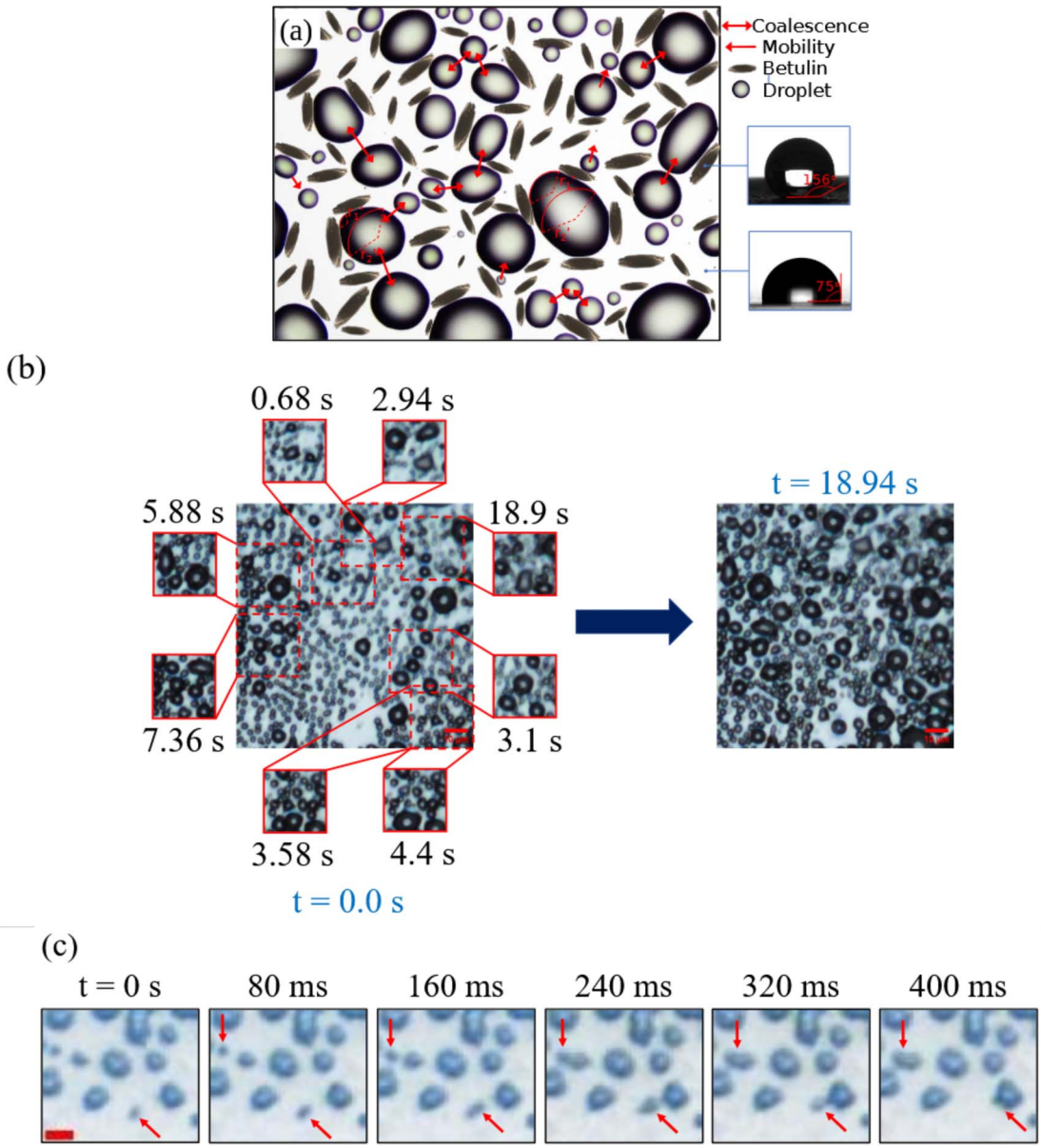

Fig. 5 (a) Illustrations depicting surface free energy gradient and Laplace pressure, induced by superhydrophobic/hydrophilic betulin microstructures, responsible for condensation, droplet mobility and coalescence. The droplets in insets demonstrate the wettabilities on the betulin surface and the particle-free substrate. (b) Micrographs exhibiting experimental microdroplet mobility and coalescence events leading to droplet growth, captured during fog harvesting on a betulin-coated surface. The dotted red boxes indicate the microdroplets that formed at various locations in the image at the reference time of $t = 0$ s. The solid red boxes illustrate the displacement and coalescence of the droplets after the time specified at the top of each box. (c) Snapshots demonstrate droplets crawling and merging into bigger droplets on a betulin-coated surface. In (b) and (c) the surfaces were perfectly horizontal and the scale bars are 10 μm.

droplet straddled between two particles. The resultant Laplace pressure gradient,

$$\Delta P = \gamma\left(\frac{1}{r_1}+\frac{1}{r_2}\right) \quad (2)$$

where r_1 and r_2 are radii of curvature at two regions of an asymmetric droplet as displayed in Fig. 5(a) and γ is the surface tension of water. The ΔP complements the $\Delta\Gamma$-induced droplet mobility and coalescence.

A typical surface mobility-induced drop growth on a Bet-LO surface is demonstrated in Fig. 5(b and c). The micrographs show the microdroplets produced through condensation on a betulin-coated surface, when exposed to humid air, and their surface free energy gradient-induced motion. The surface was perfectly horizontal such that gravity did not influence the droplet motion or growth. The evolution of droplet size at different spots is highlighted at different time steps. The image at 18.94 s clearly shows the overall drop size change in comparison with the initial droplet distribution. The growth in the intermediate time steps is presented in Fig. S3.† In the time-lapse images presented in Fig. 5(c), individual microdroplets <3 μm, can be seen moving and merging (pointed by red arrows). The droplets traveled distances equivalent to twice their size in time under a second. The merging was observed to take place at different length scales.

The motion of the water microdroplets is governed by the distribution and orientation of betulin particles at the surface. Superhydrophobic surfaces are reported to induce droplet mobility.[36] The synthetic hybrid superhydrophobic–superhydrophilic surfaces augment the surface motion.[14] We measured the time-averaged mobility (U) of water microdroplets on the betulin coatings and compared the data with the mobility on a silanized glass surface. The droplet motion captured on a smooth silanized glass surface was mainly caused by droplet dewetting upon impact. The data presented in Fig. 6 suggests that the droplets moved faster on a superhydrophobic/hydrophilic betulin surface. The mobility on Bet-LO surfaces with different betulin surface densities were found to be similar. Further, bigger droplets moved faster on the surface, although the tracked droplets were under 5 μm. The scattering of the data is attributed to the randomness in the droplet motion.

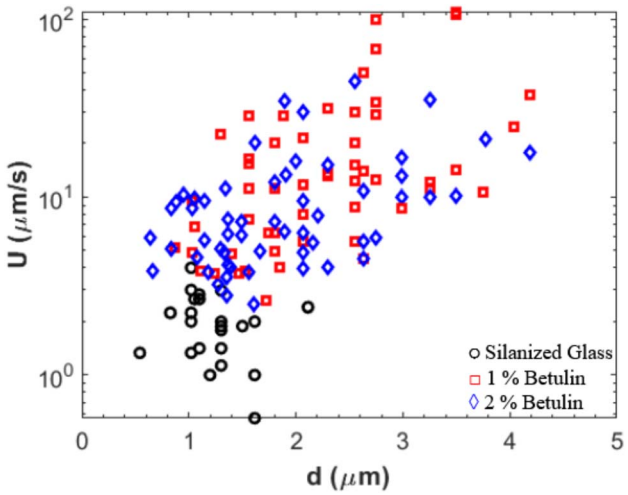

Fig. 6 The time-averaged mobility (U) of water microdroplets was measured on silanized glass and substrates coated with Bet-LO containing 1 wt% and 2 wt% betulin. The mobility was calculated by tracking the position of the droplets, with d representing the base diameter of a droplet, which is proportional to its size.

3.4 Water collection efficiency

In fog harvesting, it is crucial that the water drops formed on the collector surface are able to shed freely. The collectors are usually installed inclined such that gravity helps the water cascade along the surface. Hydrophobicity of the surface influences the drop growth and subsequent slide. By contrast, a hydrophilic surface allows a water drop spread to cover a larger area, thus limiting the sites for renewed nucleation and hindering the heat transfer. An untreated glass surface is an excellent example, where a water drop firmly holds on to the hydrophilic surface even at 90° inclination, as demonstrated in Fig. 7(a). On the contrary, a hydrophobic silanized glass surface lets the same size drop slip when tilted to 50° (Fig. 7(b)). A water drop placed on a betulin-coated surface readily pins, thanks to the roughness granted by the densely packed particles, regardless of the surface inclination. The pinning was observed in all betulin-coated surfaces in spite of the surface particle density, which is also shown in Fig. S2.† Fig. 7(c) and (d) clearly illustrate the size-dependent drop behavior on betulin coatings. A 5 μL water droplet adhered to the surface even at a steep inclination, while increasing the drop volume to 30 μL caused it to detach at 32°. The drop appeared to roll on the surface, unlike slipping on a smooth silanized glass. The fall suggests Cassie–Baxter state where a drop rests on the particles without wetting the substrate underneath.

The effects of spreading and pinning of a water droplet on surfaces with varying wettability and microstructures are evident in the images of untreated and betulin-coated glass surfaces exposed to fog, as shown in Fig. 7(e) and (f). The surface coated with 1 wt% Bet-PLA-2 promotes drop-wise condensation, allowing droplet growth to be confined to the hydrophilic area while providing ample space around the droplet for new condensation. In contrast, untreated glass exhibits film-wise condensation, where water spreads across a large portion of the surface, significantly reducing the area available for new nucleation.

The amount of water a surface allows to condense when placed in fog conditions is measured using a setup demonstrated in Fig. 8(a). A humidifier was used to create fog which also contained microdroplets under 25 μm, moving at velocities ranging from 25 mm s^{-1} to 290 mm s^{-1}, corresponding to a Reynolds number Re < 1. These parameters were similar to that of a natural fog where the droplets may vary in size, from 5 to 50 μm, and velocity between 1 and 5 cm s^{-1} depending on the

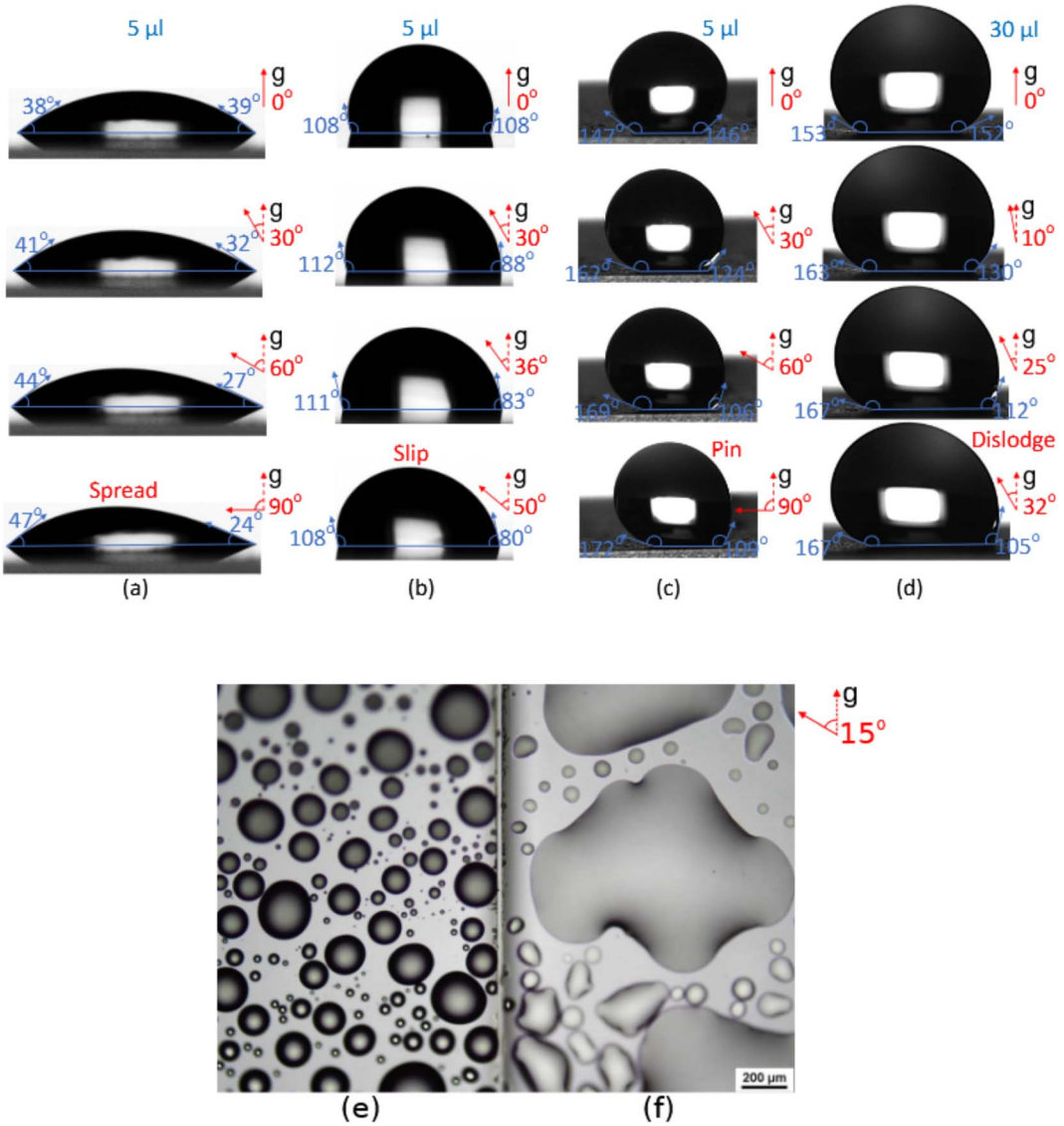

Fig. 7 Roll-off contact angles of water drop on differently coated surfaces. (a) A water drop spreads on an untreated glass surface during 0° to 90° tilting. (b) A drop on a silanized glass starts slipping when the glass is inclined to 50°. (c) A 5 µL water drop remains pinned to a Bet-PLA-2 coating containing 3 wt% betulin, but a 30 µL drop (d) easily falls off the surface when tilted to 30°. (e and f) Micrographs depicting drop-wise (e) and film-wise (f) condensation on coated (1 wt% betulin) and untreated glass, respectively. The red arrows indicate the inclination of the surface with respect to gravity, *g*. The measurements were done at room temperature.

local weather conditions.[37–39] The collector was held 45° to minimize the aerodynamic resistance and assist in the continuous rolling of bigger drops. The water shedding from the substrate was collected and measured as a time-averaged water collection rate. Unlike several fog harvesting studies in the literature, the measurements were done without passing a coolant through the collector.

The water collection rates on differently coated surfaces, presented in Fig. 8(b)–(d), show that the presence of betulin on a surface drastically increases the water collection. A bare glass which is essentially hydrophilic, condensed up to 300 mg of water over a cm^2 area in an hour. All the binder coatings (free of betulin) reduced the hydrophilicity when applied to glass and resulted in better water collection. However, a considerable rise was observed when betulin particles were present at the surface. The increase in betulin density, *i.e.*, reducing the inter-particle distance, augmented the water collection efficiency. Although the collection rate did not show dramatic growth upon increasing the betulin content in Bet-LO coatings, the overall rate was 700% and 60% higher than an uncoated glass and a silanized glass, respectively. Bet-PLA-1 and Bet-PLA-2 coatings, on the other hand, showed a sizable intensification in the water condensation and the collection upon the increase in the betulin content. However, the rate declined when betulin surface density surpassed a threshold, suggesting an optimum density. For the Bet-PLA-1 coatings, the optimum was ≈3 wt% betulin, while it was ≈2 wt% betulin in the Bet-PLA-2 coatings. Apparently, the Bet-PLA coatings performed better than Bet-LO,

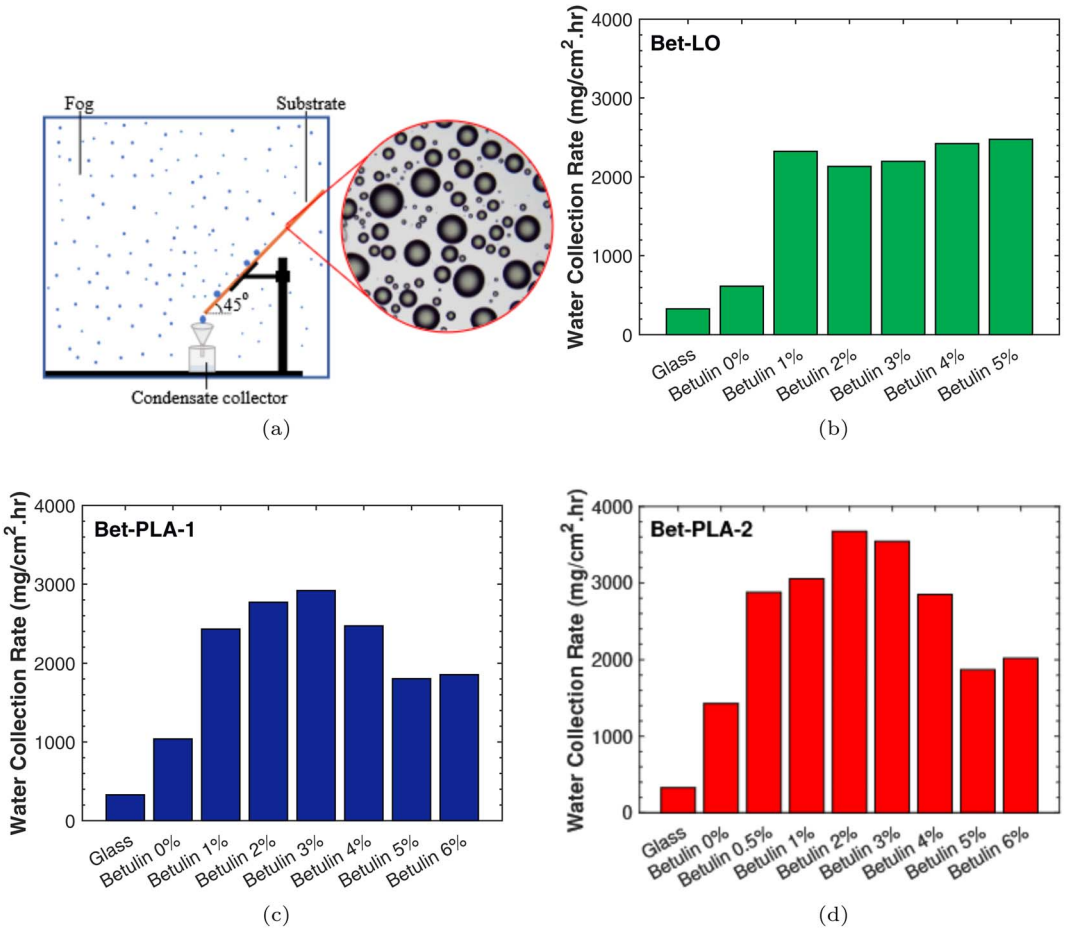

Fig. 8 (a) Schematics of the setup used to measure the water collection efficiency of betulin-coated permeable and impermeable collectors. The collectors were tilted at a 45° angle to minimize aerodynamic resistance while exposed to fog. The inset shows a micrograph of condensate droplets on a betulin-coated surface. Time-averaged water collection rates on Bet-LO (b), Bet-PLA-1 (c), and Bet-PLA-2 (d) coated on glass having different betulin areal densities. The measurements were done at room temperature, while no coolant passed through the collectors.

as the Bet-PLA-1 and Bet-PLA-2 surfaces collected 18% and 48% more water, respectively at the optimum betulin surface densities.

The water collection rates on PLA-based coatings containing >4 wt% betulin plateaued between 1800 and 2000 mg cm^{-2} h^{-1}. The rate at the higher particle density was roughly similar to that of silanized glass *i.e.* 1500 mg cm^{-2} h^{-1}. On the Bet-PLA-1 and Bet-PLA-2 coatings with >4 wt% betulin, the particles fully covered the substrate as shown in Fig. 2(c), 3(b and d). The coatings become superhydrophobic, as suggested by the contact angle data presented in Fig. 4(d), where the droplet mobility does not commensurate with the hybrid nature of the coatings at lower betulin content. All data on water collection rates were measured at different times, with each measurement repeated at least twice. The data sets for the Bet-PLA-2 coatings, recorded two months apart, are presented in Fig. S4 of the ESI.†

3.4.1 Commercial fog harvesters and a comparison with previous studies. The effectiveness of the betulin coatings on commercial fog harvesters was tested using two meshes, 35% Raschel and stainless steel (SS) meshes, shown in Fig. 9(a). The Raschel[2] and metal[6] meshes are widely used as fog collectors. As opposed to an impermeable collector such as glass, metal, and polymer sheets, the meshes apply less aerodynamic resistance to a droplet-carrying airflow. The betulin coatings with optimum particle densities, identified for the glass substrates, were spray-coated onto the meshes and allowed to dry at room temperature. Since DCM is incompatible with polymers, Bet-PLA-1 was limited to the stainless steel mesh. No further treatment was required to reinforce the coatings on the polymer and metal surfaces.

The water collection efficiencies of the bare meshes were dismal, between 300 and 400 mg cm^{-2} h^{-1}. However, the application of betulin coatings remarkably magnified the water collection rates on both meshes; the effect is apparent from the data presented in Fig. 9(b) and (c). On the Raschel mesh, both coatings – Bet-LO and Bet-PLA-2 – unquestionably boosted the water collection rate by over 255% and 270% respectively. The numbers are lower as compared to the betulin-coated

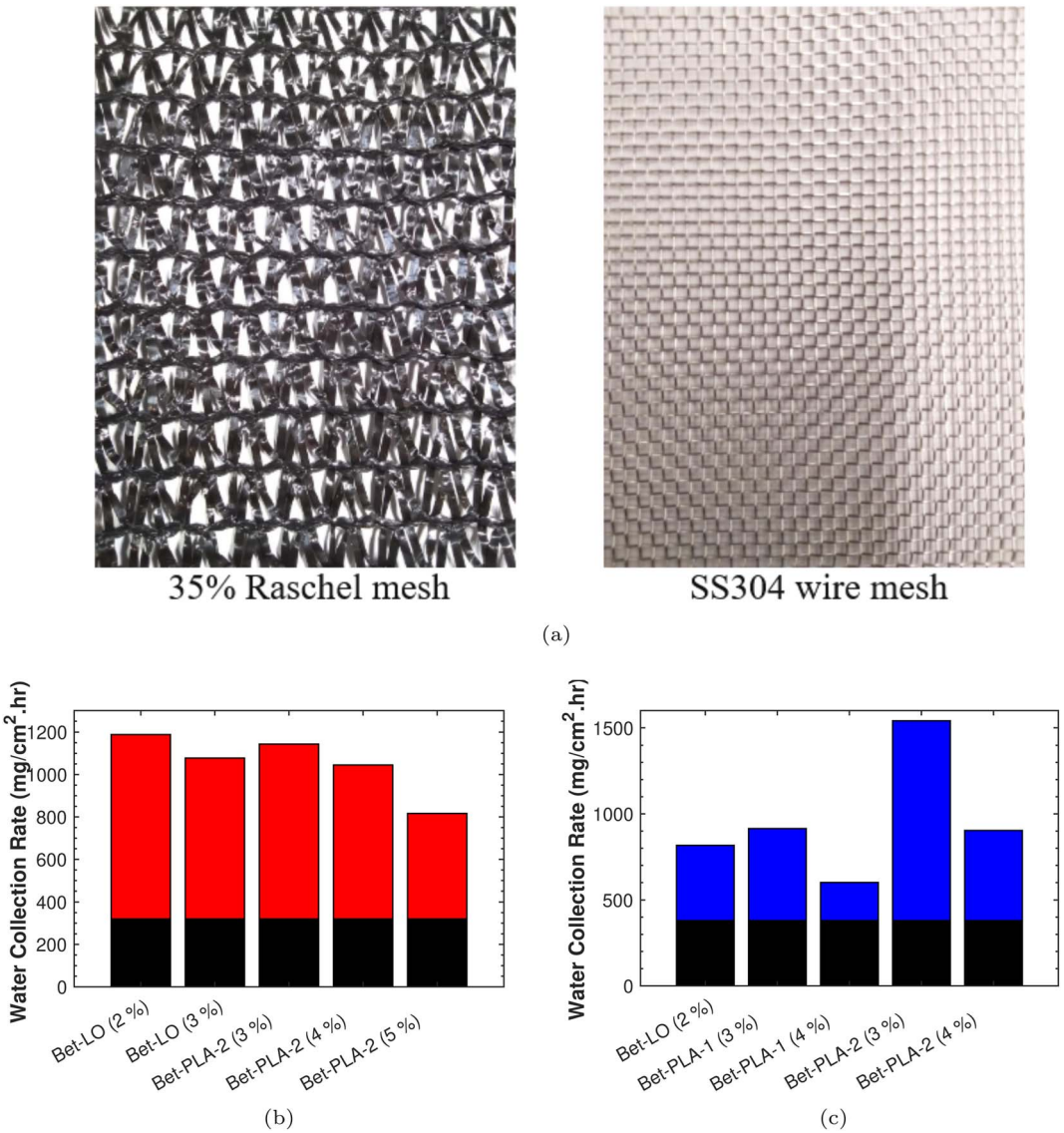

Fig. 9 (a) 35% Raschel mesh and 304 stainless steel mesh. The water collection rates measured on betulin-coated Raschel mesh (b) and stainless steel mesh (c) collectors. The lower charts (in black) show the collection rates on bare meshes. The numbers in the parentheses indicate the betulin content (wt%) of the coatings.

impermeable collectors given the lower surface area available for the condensation. Interestingly, the surface particle density-dependent efficiency trend observed for the glass collectors persisted. The coated stainless steel mesh also showed improved collection efficiency (although Bet-PLA-1 with 4 wt% betulin was an outlier), whereas Bet-PLA-2 containing 3 wt% betulin intensified the efficiency by over 300%. Furthermore, the coatings allowed swift cascading of the grown drops along the mesh surface, without blocking its pores or interrupting renewed condensation.

Table 1 presents a comprehensive summary of the water collection efficiencies of different synthetic coatings in various conditions. The collectors include commercially available meshes as well as micropatterned surfaces. The data clearly shows that among the impermeable collectors, the betulin-coated glass collectors have the edge on the reported micro-patterned fog collectors, including the star-shaped TiO_2 nano-particle patterns,[29] which reportedly gave the best condensation rate of 2780 mg cm^{-2} h^{-1}. In contrast, the water collection rates on the Bet-LO, Bet-PLA-1, and Bet-PLA-2 coated glass collectors were 2478, 2919, and 3677 mg cm^{-2} h^{-1}, respectively. The uncoated mesh collectors yield significantly lower collections (< 35 mg cm^{-2} h^{-1}), regardless of their material, design or test conditions. As the data in Table 1 demonstrates, the application of Bet-LO, Bet-PLA-1, and Bet-PLA-2 on both mesh collectors undeniably led to a remarkable increase in water collection yield. Additionally, despite the fact that condensation rates are influenced by fog conditions, the betulin-coated Raschel mesh managed to collect over double the water compared to the largest reported collection rate.[42]

Table 1 Summary of various micropatterned and commercial fog harvesters, and their water collection rates reported in the literature

No	Collector	Collection rate mg cm^{-2} h^{-1}	Test condition/location
1	35% Raschel mesh[40]	5.14	Coastal desert/Henties Bay, Namibia
2	40% Aluminet, indoor weave[40]	4.78	
3	60% Aluminet, indoor weave[40]	3.70	
4	90% Aluminet, indoor weave[40]	1.80	
5	35% Raschel mesh[41]	34.47	Hill top/Cerro Moreno, Chile
6		32.54	Seashore/Alto Patache, Chile
7		14.00	Hill top/Coastal/Paposo, Chile
8		12.42	Hill top/El Tofo, Chile
9		5.96	Seashore/Falda Verde, Chile
10		3.87	Hill top/Cerro Guatalaya, Chile
11	35% Raschel mesh[42]	358[a]	Hilltop/Masroob, Oman
12	47% Tildenet mesh[42]	26.67	Coastal mountain/Dhofar, Oman
13	50% Coresa mesh[42]	26.25	Coastal mountain/Dhofar, Oman
14	35% Raschel mesh[6]	18.75	Mountain/Hajja, Yemen
15	Double-layer 35% Raschel mesh[43]	13.94	Coastal grassland/Montara, California
16	Hydrofobised stainless steel mesh[43]	14.33	Grassland slope/Pepperwood Preserve, California
17	3-d Spacer fabric[43]	14.47	Coastal chaparral/Fritzsche Field, California
18	Nanotextured superhydrophilic single aluminum wire[44]	4000	Humidifier, lab setup
19	Hydrophobic G. *dalenii* replica[45]	185	Ultrasonic humidifier, lab setup
20	Microgrooved copper wire[46]	694	Ultrasonic humidifier, lab setup
21	Superhydrophobic polyolefin mesh[46]	200	
22	Star shape, TiO_2 nanoparticle micropatterned surface[29]	2780	Ultrasonic humidifier, lab setup
23	Inkjet printed hybrid superhydrophilic-superhydrophobic micropatterned surface[47]	62	Ultrasonic humidifier, lab setup
24	Micro-patterned hydrophobic–hydrophilic surface coatings on solid surfaces[48]	340	Humidity chamber, collector cooled below dew point
25	Micropatterned plasma-etched silicon wafer[56]	24.44	Humidity chamber, collector cooled to dew point
26	Copper wire with electrochemically induced roughness gradient[17]	618	Ultrasonic humidifier, lab setup
27	Micro/nanopatterned surface with laser-fabricated PTFE nanoparticles on superhydrophobic copper mesh[49]	200	Humidifier, lab setup
28	PDMS and diatomite-alginate-based fiber fabricated using droplet microfluidics and 3D printing[50]	750	Ultrasonic humidifier, lab setup
29	Magnetic particle-assisted molding-based conical microtips[b] [51]	7–9 μg s^{-1}	Ultrasonic humidifier, lab setup
	This work		
	Bet-LO		
	Glass	2478	
	35% Raschel mesh	868	
	Stainless steel mesh	437	
	Bet-PLA-1		
	Glass	2919	
	Stainless steel mesh	535	
	Bet-PLA-2		
	Glass	3677	
	35% Raschel mesh	823	
	Stainless steel mesh	1161	

[a] Fog and drizzle. [b] Measured on single tip.

4 Conclusions

Microtextured surfaces with naturally superhydrophobic betulin particles not only promote condensation but also induce autonomous movement of water microdroplets when exposed to fog. These phenomena are due to the combined superhydrophobic and hydrophilic properties of the betulin coated surfaces. The movement of the microdroplets on the surface is attributed to a surface free energy gradient ($\Delta\Gamma$), which is created by the superhydrophobic particle surfaces and the hydrophilic gaps between the particles. The $\Delta\Gamma$ of a coating depends on betulin particles' areal density, where higher density results in superhydrophobicity and a Cassie state. Different binders used to apply the betulin particles to substrates influence the morphology and microstructure of the surfaces. By identifying the optimal particle density in each coating, it was observed that water droplet mobility and water collection efficiency were enhanced. This improvement was found to be up to 10 times on impermeable substrates, depending on the binder mixture. When applied to commercial fog harvesting meshes, the efficiency was increased by 2.5 to 3 times compared to the bare meshes.

The plant-based particle coatings presented in this study are environmentally friendly, sustainable, and simple to use in fog harvesting applications, unlike the micro/nano-patterned synthetic materials. Scientific efforts to create synthetic superhydrophobic and hybrid superhydrophobic/superhydrophilic surfaces through micropatterning have limitations in water harvesting. First, the intricate structures are not practical to apply on large flexible surfaces typically used in fog harvesting. Second, the synthetic materials used are costly and derived from unsustainable sources. Third, the surfaces are prone to defects. However, scabrous yet microscopically textured structures created by using betulin particles provided the necessary roughness as well as the hybrid superhydrophobic/hydrophilic properties required for condensation and droplet mobility.

Data availability

The data supporting this article have been included as part of the ESI.†

Conflicts of interest

There are no conflicts to declare.

Acknowledgements

The authors acknowledge funding from the Canada Excellence Research Chair Program (CERC-2018-00006) and the Canada Foundation for Innovation (Project number 38623). The authors are also thankful to the UBC Centre for High-Throughput Phenogenomics facility for access to SEM.

References

1 R. S. Schemenauer and P. Cereceda, Fog-Water Collection in Arid Coastal Locations, *Ambio*, 1991, **20**, 303–308.
2 O. Klemm, *et al.*, Fog as a Fresh-Water Resource: Overview and Perspectives, *Ambio*, 2012, **41**, 221–234.
3 R. Ghosh, T. K. Ray and R. Ganguly, Cooling tower fog harvesting in power plants – A pilot study, *Energy*, 2015, **89**, 1018–1028.
4 M. Azeem, M. T. Noman, J. Wiener, M. Petru and P. Louda, Structural design of efficient fog collectors: A review, *Environ. Technol. Innovation*, 2020, **20**, 101169.
5 W. Shi, M. J. Anderson, J. B. Tulkoff, B. S. Kennedy and J. B. Boreyko, Fog Harvesting with Harps, *ACS Appl. Mater. Interfaces*, 2018, **10**, 11979–11986.
6 S. A. Abdul-Wahab, A. M. Al-Damkhi, H. Al-Hinai, K. A. Al-Najar and M. S. Al-Kalbani, Total fog and rainwater collection in the Dhofar region of the Sultanate of Oman during the monsoon season, *Water Int.*, 2010, **35**, 100–109.
7 J. Rivera, Aerodynamic collection efficiency of fog water collectors, *Atmos. Res.*, 2011, **102**, 335–342.
8 C. Fang, J. E. Steinbrenner, F.-M. Wang and K. E. Goodson, Impact of wall hydrophobicity on condensation flow and heat transfer in silicon microchannels, *J. Manuf. Syst.*, 2010, **20**, 045018.
9 S. Anand and S. Y. Son, Sub-Micrometer Dropwise Condensation under Superheated and Rarefied Vapor Condition, *Langmuir*, 2010, **26**, 17100–17110.
10 Bejan, A., Kraus, A. D., ed. *Heat Transfer Handbook*; Wiley-Interscience: New Jersey, 2003.
11 S. Daniel, M. K. Chaudhury and J. C. Chen, Fast Drop Movements Resulting from the Phase Change on a Gradient Surface, *Science*, 2001, **291**, 633–636.
12 J. W. Rose, Dropwise condensation theory and experiment: A review, *Proc. Inst. Mech. Eng., Part A*, 2002, **216**, 115–128.
13 S. Parvate, P. Dixit and S. Chattopadhyay, Superhydrophobic Surfaces: Insights from Theory and Experiment, *J. Phys. Chem. B*, 2020, **124**, 1323–1360.
14 S. Anand, A. T. Paxson, R. Dhiman, J. D. Smith and K. K. Varanasi, Enhanced Condensation on Lubricant-Impregnated Nanotextured Surfaces, *ACS Nano*, 2012, **6**, 10122–10129.
15 Y. Wang, W. Zhao, M. Han, J. Xu and K. Tam, Biomimetic surface engineering for sustainable water harvesting systems, *Nat. Water*, 2023, **1**, 587–601.
16 D. Hua, Z. Yongmei, W. Nü, B. Hao, W. Li, W. Jing, Z. Yong and J. Lei, Highly Efficient Fog Collection Unit by Integrating Artificial Spider Silks, *Adv. Mater. Interfaces*, 2016, **3**, 1500831.
17 L. Y. Zhang, Z. Xu and J. H. Masliyah, Langmuir and Langmuir-Blodgett films of mixed asphaltene and a demulsifier, *Langmuir*, 2003, **19**, 9730–9741.
18 C. T. Schriner and B. Bhushan, Water droplet dynamics on bioinspired conical surfaces, *Philos. Trans. R. Soc., A*, 2019, **377**, 20190118.
19 Y. Zheng, H. Bai, Z. Huang, X. Tian, F.-Q. Nie, Y. Zhao, J. Zhai and L. Jiang, Directional water collection on wetted spider silk, *Nature*, 2010, **463**, 640–643.
20 H. Bai, J. Ju, R. Sun, Y. Chen, Y. Zheng and L. Jiang, Controlled Fabrication and Water Collection Ability of

Bioinspired Artificial Spider Silks, *Adv. Mater.*, 2011, **23**, 3708–3711.

21 J. Guadarrama-Cetina, A. Mongruel, M. G. Medici, E. Baquero, A. R. Parker, I. Milimouk-Melnytchuk, W. Gonzalez-Vinas and D. Beysens, Dew condensation on desert beetle skin, *Eur. Phys. J. E*, 2014, **37**, 109.

22 B. White, A. Sarkar and A.-M. Kietzig, Fog-harvesting inspired by the Stenocara beetle—An analysis of drop collection and removal from biomimetic samples with wetting contrast, *Appl. Surf. Sci.*, 2013, **284**, 826–836.

23 Z. Xinjuan, Q. Long, Y. Xianxia, Z. Cailong, L. Zhaowen, C. Jiang, X. Shouping, W. Shuangfeng, P. Pihui and W. Xiufang, Inspired by Stenocara Beetles: From Water Collection to High-Efficiency Water-in-Oil Emulsion Separation, *ACS Nano*, 2017, **11**, 760–769.

24 Y. Lai, X. Gao, H. Zhuang, J. Huang, C. Lin and L. Jiang, Designing Superhydrophobic Porous Nanostructures with Tunable Water Adhesion, *Adv. Mater.*, 2009, **21**, 3799–3803.

25 H. Notsu, W. Kubo, I. Shitanda and T. Tatsuma, Super-hydrophobic/super-hydrophilic patterning of gold surfaces by photocatalytic lithography, *J. Mater. Chem.*, 2005, **15**, 1523–1527.

26 X. Guo and X. Li, An expanding horizon: Facile fabrication of highly superhydrophobic coatings, *Mater. Lett.*, 2017, **186**, 357–360.

27 B.-B. Wang, X.-D. Wang, W.-Y. Yan and T.-H. Wang, Molecular dynamics simulations on coalescence and non-coalescence of conducting droplets, *Langmuir*, 2015, **31**, 7457–7462.

28 R. Ghosh, R. P. Sahu, R. Ganguly, I. Zhitomirsky and I. K. Puri, Photocatalytic activity of electrophoretically deposited TiO2 and ZnO nanoparticles on fog harvesting meshes, *Ceram. Int.*, 2020, **46**, 3777–3785.

29 H. Bai, L. Wang, J. Ju, R. Sun, Y. Zheng and L. Jiang, Efficient Water Collection on Integrative Bioinspired Surfaces with Star-Shaped Wettability Patterns, *Adv. Mater.*, 2014, **26**, 5025–5030.

30 A. Steele, I. Bayer, S. Moran, A. Cannon, W. P. King and E. Loth, Conformal ZnO nanocomposite coatings on micro-patterned surfaces for superhydrophobicity, *Thin Solid Films*, 2010, **518**, 5426–5431.

31 H. Yang and P. Jiang, Scalable fabrication of superhydrophobic hierarchical colloidal arrays, *J. Colloid Interface Sci.*, 2010, **352**, 558–565.

32 D. K. Owens and R. C. Wendt, Estimation of the surface free energy of polymers, *J. Appl. Polym. Sci.*, 1969, **13**, 1741–1747.

33 Y. Guan, C. Yu, J. Zhu, R. Yang, X. Li, D. Wei and X. Xu, Design and fabrication of vapor-induced superhydrophobic surfaces obtained from polyethylene wax and silica nanoparticles in hierarchical structures, *RSC Adv.*, 2018, **8**, 25150–25158.

34 A. Marmur, Wetting on Hydrophobic Rough Surfaces: To Be Heterogeneous or Not To Be?, *Langmuir*, 2003, **19**, 8343–8348.

35 F. M. Fowkes, Attractive forces at interfaces, *Ind. Eng. Chem.*, 1964, **56**, 40–52.

36 J. B. Boreyko and C.-H. Chen, Self-Propelled Dropwise Condensate on Superhydrophobic Surfaces, *Phys. Rev. Lett.*, 2009, **103**, 184501.

37 R. S. Schemenauer and P. I. Joe, The collection efficiency of a massive fog collector, *Atmos. Res.*, 1989, **24**, 53–69.

38 R. S. Schemenauer and P. Cereceda, Fog collection's role in water planning for developing countries, *Nat. Resour. Forum*, 1994, **18**, 91–100.

39 A. L. Igel and S. C. van den Heever, The Importance of the Shape of Cloud Droplet Size Distributions in Shallow Cumulus Clouds. Part I: Bin Microphysics Simulations, *J. Atmos. Sci.*, 2017, **74**, 249–258.

40 E. S. Shanyengana, R. D. Sanderson, M. K. Seely and R. S. Schemenauer, Testing greenhouse shade nets in collection of fog for water supply. J. Water Supply, *Aqua*, 2003, **52**, 237–241.

41 H. Larrain, F. Velasquez, P. Cereceda, R. Espejo, R. Pinto, P. Osses and R. S. Schemenauer, Fog measurements at the site "Falda Verde" north of Chañaral compared with other fog stations of Chile, *Atmos. Res.*, 2002, **64**, 273–284.

42 R. S. Schemenauer and P. A. Cereceda, Proposed Standard Fog Collector for Use in High-Elevation Regions, *J. Appl. Meteorol. Climatol.*, 1994, **33**, 1313–1322.

43 D. M. Fernandez, A. Torregrosa, P. S. Weiss-Penzias, B. J. Zhang, D. Sorensen, R. E. Cohen, G. H. McKinley, J. Kleingartner, A. Oliphant and M. Bowman, Fog Water Collection Effectiveness: Mesh Intercomparisons, *Aerosol Air Qual. Res.*, 2018, **18**, 270–283.

44 Y. Jiang, S. Savarirayan, Y. Yao and K.-C. Park, Fog collection on a superhydrophilic wire, *Appl. Phys. Lett.*, 2019, **114**, 083701.

45 V. Sharma, D. Orejon, Y. Takata, V. Krishnan and S. Harish, Gladiolus dalenii Based Bioinspired Structured Surface *via* Soft Lithography and Its Application in Water Vapor Condensation and Fog Harvesting, *ACS Sustainable Chem. Eng.*, 2018, **6**, 6981–6993.

46 M. A. K. Azad, D. Ellerbrok, W. Barthlott and K. Koch, Fog collecting biomimetic surfaces: Influence of microstructure and wettability, *Bioinspiration Biomimetics*, 2015, **10**, 016004.

47 L. Zhang, J. Wu, M. N. Hedhili, X. Yang and P. Wang, Inkjet printing for direct micropatterning of a superhydrophobic surface: toward biomimetic fog harvesting surfaces, *J. Mater. Chem. A*, 2015, **3**, 2844–2852.

48 S. C. Thickett, C. Neto and A. T. Harris, Biomimetic Surface Coatings for Atmospheric Water Capture Prepared by Dewetting of Polymer Films, *Adv. Mater.*, 2011, **23**, 3718–3722.

49 K. Yin, H. Du, X. Dong, C. Wang, J.-A. Duan and J. He, A simple way to achieve bioinspired hybrid wettability surface with micro/nanopatterns for efficient fog collection, *Nanoscale*, 2017, **9**, 14620–14626.

50 P. Zhu, R. Chen, C. Zhou, Y. Tian and L. Wang, Asymmetric fibers for efficient fog harvesting, *Chem. Eng. J.*, 2021, **415**, 128944.

51 M. Cao, J. Ju, K. Li, S. Dou, K. Liu and L. Jiang, Facile and Large-Scale Fabrication of a Cactus-Inspired Continuous Fog Collector, *Adv. Funct. Mater.*, 2014, **24**, 3235–3240.

52 P. Siman, A. Filipova, A. Ticha, M. Niang, A. Bezrouk and R. Havelek, Effective Method of Purification of Betulin from Birch Bark: The Importance of Its Purity for Scientific and Medicinal Use, *PLoS One*, 2016, **11**, 1–14.
53 T. Huang, C. Chen, D. Li and M. Ek, Hydrophobic and antibacterial textile fibres prepared by covalently attaching betulin to cellulose, *Cellulose*, 2019, **26**, 665–677.
54 X. Niu, H. Zhu, S. Mhatre, R. Bi, Y. Ye and O. J. Rojas, Betulin Enables Multifunctional Cellulose-Based Insulative Foams with Low Environmental Impacts, *ACS Nano*, 2024, **18**(31), 20247–20257.
55 D. Gurera and B. Bhushan, Designing bioinspired surfaces for water collection from fog, *Philos. Trans. R. Soc., A*, 2019, **377**, 20180269.
56 A. Lee, M.-W. Moon, H. Lim, W.-D. Kim and H.-Y. Kim, Water harvest *via* dewing, *Langmuir*, 2012, **28**, 10183–10191.